NANO LETTERS

Letter

pubs.acs.org/NanoLett

Electronic Transport of Encapsulated Graphene and WSe_2 Devices Fabricated by Pick-up of Prepatterned hBN

Joel I-Jan Wang,*[,†] Yafang Yang,*[,‡] Yu-An Chen,[‡] Kenji Watanabe,[§] Takashi Taniguchi,[§] Hugh O. H. Churchill,[‡] and Pablo Jarillo-Herrero*[,‡]

[†]School of Engineering and Applied Sciences, Harvard University, 29 Oxford Street, Cambridge, Massachusetts 02138, United States

[‡]Department of Physics, Massachusetts Institute of Technology, 77 Massachusetts Avenue, Cambridge, Massachusetts 02139, United States

[§]National Institute for Materials Science, Namiki 1-1, Tsukuba, Ibaraki 305-0044, Japan

Supporting Information

ABSTRACT: We report high quality graphene and WSe_2 devices encapsulated between two hexagonal boron nitride (hBN) flakes using a pick-up method with etched hBN flakes. Picking up prepatterned hBN flakes to be used as a gate dielectric or mask for other 2D materials opens new possibilities for the design and fabrication of 2D heterostructures. In this Letter, we demonstrate this technique in two ways: first, a dual-gated graphene device that is encapsulated between an hBN substrate and prepatterned hBN strips. The conductance of the graphene device shows pronounced Fabry−Pérot oscillations as a function of carrier density, which implies strong quantum confinement and ballistic transport in the locally gated region. Second, we describe a WSe_2 device encapsulated in hBN with the top hBN patterned as a mask for the channel of a Hall bar. Ionic liquid selectively tunes the carrier density of the contact region of the device, while the hBN mask allows independent tunability of the contact region for low contact resistance. Hall mobility larger than 600 $cm^2/(V\cdot s)$ for few-layer p-type WSe_2 at 220 K is measured, the highest mobility of a thin WSe_2 device reported to date. The observations of ballistic transport in graphene and high mobility in WSe_2 confirm pick-up of prepatterned hBN as a versatile technique to fabricate ultraclean devices with high quality contact.

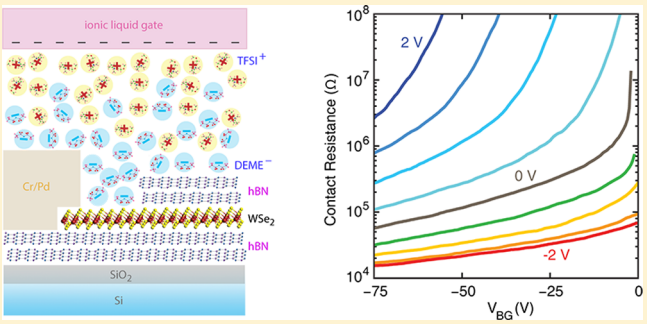

KEYWORDS: *Pick-up technique, two-dimensional (2D) heterostructures, graphene, transition metal dichalcogenides (TMDs), contact, mobility*

Two-dimensional heterostructures, composed of atomically thin layers of van der Waals materials including graphene, hBN, MoS_2, and WSe_2, among others, have drawn increasing attention in various fields for their potential to be promising platforms to study mesoscopic physics, as well as a harbinger of next generation electronics.[1] Graphene with its gapless band structure and linear dispersion provides the opportunity to study Dirac Fermions in a solid-state system, which manifests various new physics including novel quantum Hall effect, Klein tunneling, and quantum spin Hall effect.[2−6] The isolation of monolayer graphene by mechanical exfoliation has also incubated an entire set of techniques, compatible with existing nanofabrication technology that can be readily applied to other 2D van der Waals materials.[1] One interesting example is the transition metal dichalcogenides (TMDs) such as tungsten diselenide (WSe_2), an atomically layered semiconductor.[7] Few-layer TMDs have already displayed many novel nanoelectronic and optoelectronic phenomena such as ambipolar and high quality field effect transistors,[8−11] integrated circuits,[12] phototransistors[13] with high responsivity,[14] giant spin-valley coupling,[15] optical control of valley polarization[16,17] and coherence,[18] spin-layer locking in optical orientation,[19] lateral PN junctions and light-emitting diodes,[20−23] and valley Hall effect.[24] In addition to graphene and TMDs, hBN, with a large band gap of 5.5 eV, has already been used as an ideal substrate and gate dielectric for high quality graphene devices because of its atomically flat surface and nearly defect free single crystal structure.[25]

The 2D nature of these materials makes the electronic system highly accessible to external manipulation. However, the electronic properties and performance of devices based on these materials can be dictated by how much the surface properties deviate from ideal after fabrication. Previous work on graphene has shown that sample disorder can be greatly reduced via isolation from charge impurities in the substrate by means of suspension[26,27] or by building devices on ultraflat

Received: December 10, 2014
Revised: February 5, 2015
Published: February 5, 2015

DOI: 10.1021/nl504750f
Nano Lett. 2015, 15, 1898−1903

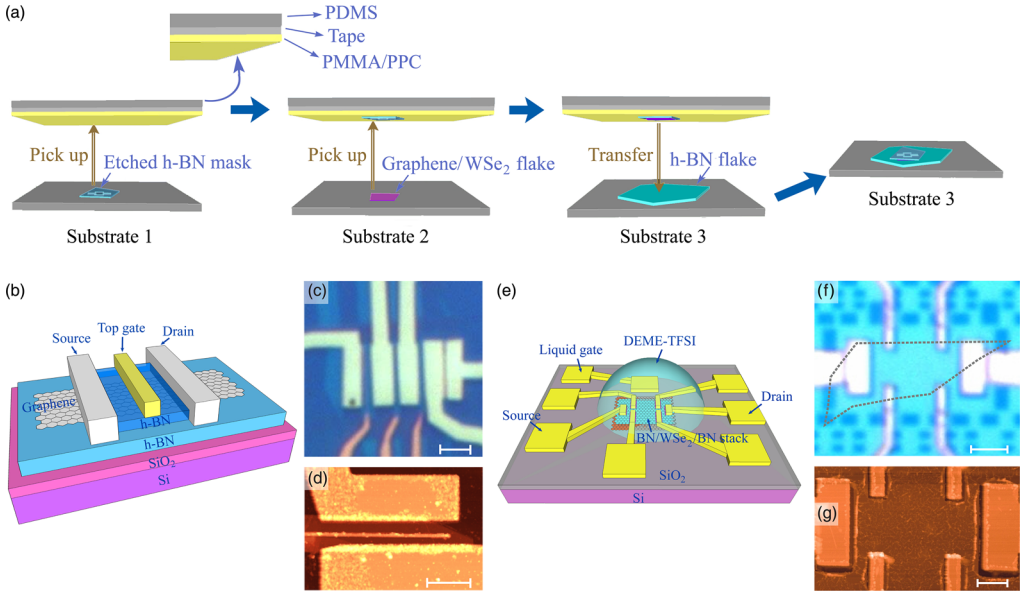

Figure 1. (a) Schematic of pick-up technique for fabrication of encapsulated devices with etched hBN on top. (b) Schematic of Sample A, a dual-gated graphene device encapsulated between hBN flakes using pick-up and transfer method. (c) Optical and (d) AFM image of the graphene device with Ti/Al leads and Au top gate on the hBN encapsulating layer. The scale bar in (c,d) is 2 and 1 μm, respectively. (e) Schematic of device structure and (f) optical, (g) AFM image of Sample B, which is a BN/WSe_2/hBN heterostructure. The top hBN is etched with Hall bar patterns. The contact leads (Cr/Pd) are slightly smaller than the holes in the top hBN to allow ionic liquid tuning of the contact region. The scale bar of (f,g) is 2 and 1 μm, respectively, and the outline of the shape of WSe_2 in (f) is drawn by superposition with the optical image of $WSe2_2$ flake before pick-up.

substrates such as hexagonal boron nitride (hBN),[25] combined with thermal or current annealing to remove fabrication residues. Additionally, encapsulation of graphene between two hBN films also leads to high quality graphene devices in which micrometer-scale ballistic transport persists up to room temperature.[28,29] The atomically flat surfaces and small lattice mismatch between both crystals facilitate strong adhesion between graphene and hBN, so that the graphene is securely sealed against contaminants derived from nanofabrication. This advantage extends to TMDs, as recent work on hBN-encapsulated MoS_2 also reveals ultrahigh low-temperature mobility up to 34 000 $cm^2/(V{\cdot}s)$ for six-layer and 1000 $cm^2/(V{\cdot}s)$ for CVD grown monolayer MoS_2.[30]

For TMDs, several methods have been explored to reduce contact resistance, including different choices of metal,[31−33] chemical doping of the contact region,[34] and graphene contacts.[30,35] We previously reported that increasing carrier density significantly diminishes the contact resistance and Schottky barriers formed at the interface of metal and MoS_2.[10] As we show below, encapsulation with patterned hBN provides the opportunity to improve device performance by independently tuning carrier density in the channel as well as in the contact region.

In previous encapsulated graphene devices, electric contact to the active layer is made by transferring exfoliated hBN flake of appropriate size and shape or by encapsulating the graphene entirely in hBN films followed by dry etching to make contacts from sides.[28,36] Here we report a scheme to make encapsulated devices by picking up and transferring a prepatterned hBN "mask". Two samples made by this method are presented: one is a dual-gated graphene device with ballistic transport in a locally gated region, and the other is a WSe_2 device in which the carrier density can be tuned independently in the channel and in the contact region. These structures provide prototypes for ballistic graphene devices and high-quality TMD devices with nearly transparent contacts, which we expect to significantly benefit the study of 2D materials in general.

Fabrication of encapsulated devices starts by preparing a prepatterned hBN mask, which seals the bulk of 2D materials under investigation while allowing metal contacts through openings in the mask. To fabricate the mask, hBN is exfoliated onto a Piranha-cleaned SiO_2/Si substrate and patterned by e-beam lithography to define the area for etching. Reactive ion etching, using CF_4, CHF_3, and H_2 as the main etching medium, is then applied to etch out hBN in exposed areas at the rate of ∼1.4 nm/second. The substrate is then submerged in acetone to remove the polymer mask and cleaned by thermal annealing in Ar/H_2 forming gas at 350 °C for 3 h.

The hBN flake can be then picked up from SiO_2 substrate by various polymers.[36,37] Here we present two samples that exemplify two of these polymers to fit different needs. Sample A is made by using PMMA to pick up patterned hBN (0.85 × 3 μm rectangle, 10 nm thick), followed by transfer onto a graphene/hBN stack prepared by a dry transfer method described previously.[38] While PMMA as pick-up agent works reliably for patterned hBN (about 70% yield) and offers the possibility to do e-beam lithography without removing the polymer in solvent, polymers with higher adhesion are required for higher-yield sequential pick-up in order to make more complex heterostructures. Therefore, for Sample B, polypropylene carbonate (PPC, 15% dissolved in anisole) is used to pick up Hall-bar patterned hBN and WSe_2 flakes successively, followed by transfer onto another hBN flake. Figure 1a shows a schematic of this pick-up process.

The pick-up process begins with preparation of transfer slides. A piece of PDMS elastomer is laid down on a glass slide, followed by 10 min UV ozone treatment. A layer of clear tape then covers the PDMS before spin coating the polymer (PMMA/PPC) and baking. The polymer/tape/PDMS is then cut into small squares and transferred onto a glass slide for

DOI: 10.1021/nl504750f
Nano Lett. 2015, 15, 1898−1903

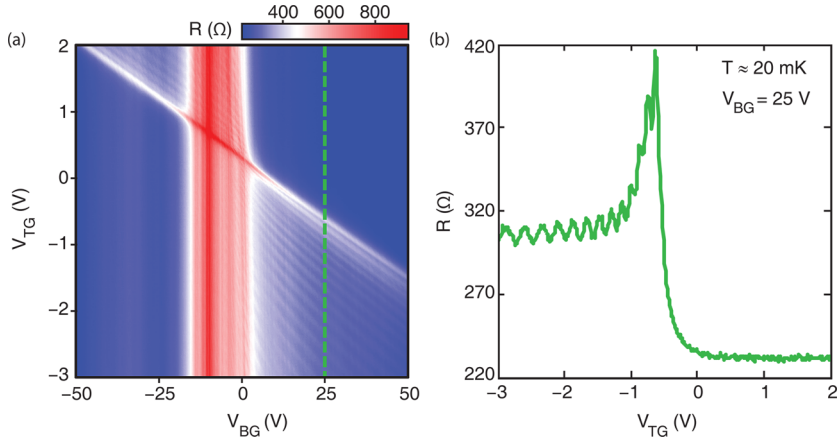

Figure 2. (a) Resistance of the graphene device as a function of top-gate and back-gate voltage. The oscillations in the n-p-n and p-n-p regions due to Klein tunneling suggest the ballistic nature of electronic transport in the locally gated region. (b) Resistance as a function of top-gate voltage while the back-gate voltage is held fixed at 25 V. The resistance oscillations observed in the n-p-n region (n-doped by the back gate and p-doped by the top gate) agree with a Fabry–Pérot model with a cavity length ∼100 nm (see text).

individual pick-up and transfer. Using an optical microscope and micromanipulators, the polymer slide is aligned with the target hBN mask at room temperature, brought into contact, and heated up to a pick-up temperature (100 °C for PMMA and 30 °C for PPC). When the polymer conforms uniformly to the surface, we lift the slide to disengage it from the substrate with a quick movement that increases the chance of pick-up. For the PPC process, we proceed to pick up another 2D material (a WSe_2 flake for Sample B) in the same way.

For the final transfer step, the polymer slide with flake(s) picked-up is pressed onto the target substrate (containing graphene/hBN for Sample A and hBN for Sample B). To release the polymer, the substrate is heated to a release temperature (140 °C for PMMA, 70 °C for PPC) and the glass slide is then raised slowly. In this way, the stack of flakes is transferred onto the substrate along with the polymer, which is subsequently dissolved in acetone or chloroform. Specific procedures for different polymers vary slightly and details for each heterostructure are described in the Supporting Information. After completion of the heterostructures, contact leads and top gates are fabricated with standard e-beam lithography and either thermal or e-beam evaporation. Details for each device are also described in the Supporting Information.

Sample A is measured in a dilution refrigerator at both 4 K and the base temperature of ≈20 mK. We discuss measurements taken on the longest (leftmost) junction in Figure 1c, which is 2.8 μm long and 0.85 μm wide. The polarities, p-type or n-type, of the entire graphene sheet and the locally gated region can be tuned individually by arbitrary combinations of a global back-gate votlage V_{BG} and a local top-gate voltage V_{TG}. These combinations result in p-n-p, n-p-n, p-p′-p, or n-n′-n junctions[39−41] as sketched in the 2D resistance map (Figure 2a). In the bipolar regime (p-n-p or n-p-n), potential barriers at two p-n interfaces define a cavity that partly confines the charge carriers inside the locally gated region. For Dirac Fermions in graphene, transport through the barriers occurs via Klein tunneling across the p-n interface, regardless of the barrier height and width,[4] while the transmission of a massive Fermion decays exponentially with the dimensions of the barrier. This gate-defined cavity is an electronic analog of the Fabry–Pérot interferometer in which the phase difference between two successive transmitted waves is $\Delta\phi = 2kL_{cavity}\cos\theta$, where L_{cavity} is the length of cavity, k is the wave vector, and θ is the angle of incidence with respect to the interface normal.[42] In graphene devices, the Fermi wave vector k_F is tuned by gating, while the dimension of the top gate mainly determines L_{cavity}. The resonance condition for conductance in a gate-tunable p-n-p junction is therefore $\Delta kL_{cavity} = \pi$, which can be expressed as $\Delta n = (2(\pi n)^{1/2})/L_{cavity}$, where $n = \pm k^2/\pi$ is the carrier density.[5,43−45]

From the resistance oscillations in Figure 2b, the peak separation in resistance around the Dirac point corresponds to $\Delta n \approx 10^{10}$ cm^{-2} at a gate voltage where $n \approx 10^{11}$ cm^{-2}. The effective cavity length L_{cavity} for our device is therefore ≈100 nm, which is in good agreement with the geometrical width of the top gate. A line-cut of the 2D gate-voltage map of resistance at V_{BG} = 25 V in Figure 2b shows that the amplitude of oscillations is almost independent of the potential difference across the p-n interface, set by $|V_{TG} - V_{BG}|$, as expected for Klein tunneling of Dirac Fermions. This quantum interference observed in the bipolar regime requires ballistic transport of charge carriers in the locally gated region, which is defined by the top-gate electrode placed on top of the transferred hBN mask. We note that the visibility of the oscillations in resistance due to Klein tunneling is significantly higher than in previous work[5] even for this relatively wide barrier (∼100 nm) due to the high quality of graphene/hBN heterostructure. Because of the limitation in geometry, we are able to do only two-probe measurement, which includes the contact resistance and the potential profile around the locally gated region. In order to extract more information about the disorder in graphene, we subtract the resistance measured at high carrier density, where we assume the contact resistance is much larger than the graphene resistance and depends weakly on carrier density[46] from the measurement and estimate the lower bound of the mobility μ to range from 8000 cm^2/(V·s) to 22 000 cm^2/(V·s). Using a semiclasscal relation between the mobility and the mean free path l, $en\mu = 2e^2k_Fl/h$, where $k_F = (\pi n)^{1/2}$,[47] we estimate the lower bound of $l \sim 390$ nm. This length is comparable to the longest distance from the lead to the edge of locally gated region. Based on the mean free path estimation and the resistance oscillation in the locally gated region, we believe the device is ballistic. The upper bound for the contact resistance is ∼330 Ω·μm, estimated from the resistance at high carrier density.

DOI: 10.1021/nl504750f
Nano Lett. 2015, 15, 1898−1903

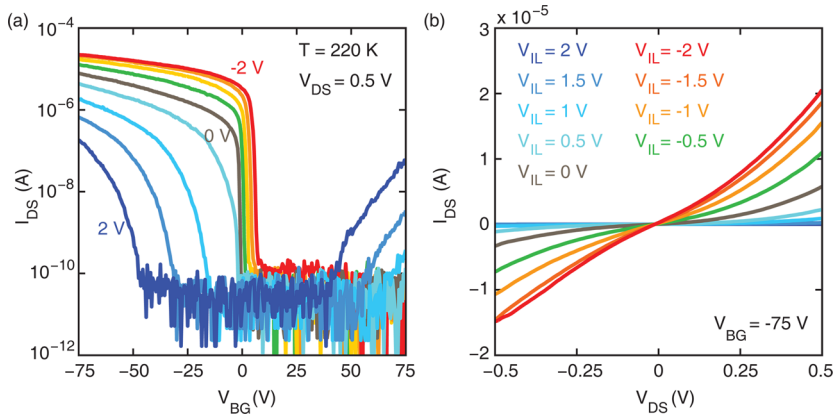

Figure 3. I_{DS} as a function of V_{BG} measured at different ionic liquid gate voltages: V_{IL} = 2, 1.5, 1, 0.5, 0, −0.5, −1, −1.5, −2 V. V_{DS} = 0.5 V. (b) I_{DS} as a function of V_{DS} for the same set of V_{IL} with fixed V_{BG} = −75 V. The temperature for all measurements was 220 K.

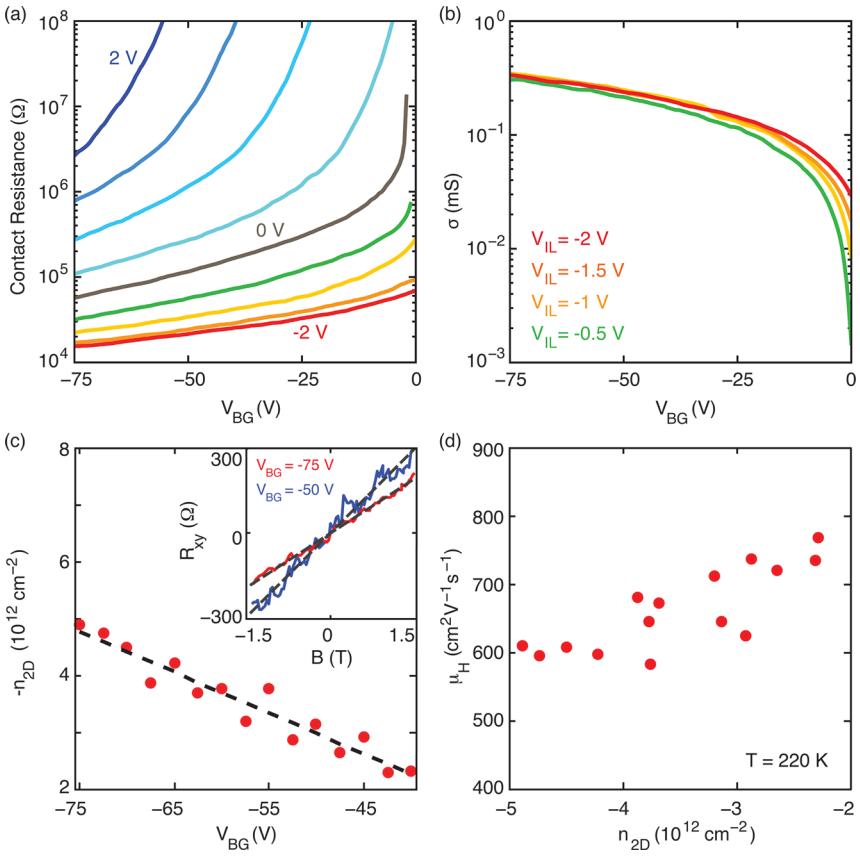

Figure 4. (a) Contact resistance as a function of V_{BG} of the WSe_2 device at different V_{IL} (denoted with the same set of colors as Figure 3). (b) Conductivity of the device as a function of V_{BG}, extracted from four-probe measurements with different ionic liquid gate voltage V_{IL} = −2 to −0.5 V, while V_{DS} = 0.5 V. (c) Carrier density calculated from Hall measurements as a function of V_{BG}. The nearly linear dependence of n_{2D} on V_{BG} corresponds to a capacitance per unit area of c = 12 nF/cm^2. Inset: selected Hall resistance versus magnetic field with V_{BG} = −75 V, −50 V. (d) Hall mobility calculated by $\mu_H = \sigma/(ne)$ is plotted against carrier density. V_{IL} = −2 V and the temperature is ∼220 K.

Sample B is a trilayer WSe_2 device encapsulated by two hBN flakes (thickness of top and bottom hBN are 35 and 25 nm respectively). The WSe_2 is contacted with Cr/Pd (0.7/100 nm) by e-beam evaporation. In addition to the hBN encapsulation introduced previously, the ionic liquid *N*,*N*-diethyl- *N*-(2-methoxyethyl)-*N*-methylammonium bis-(trifluoromethylsulfonyl-imide) (DEME-TFSI) is used to further improve the quality of the contact. When designing contacts to the device, the contact metal is patterned slightly smaller than the patterned openings in the top hBN flake (see AFM image of the device in Figure 1g), so the WSe_2 near the contact region is exposed to allow ionic liquid gating. A side-gate electrode for the ionic liquid is patterned near the flake with an area at least 100 times larger than the WSe_2 flake. After the device fabrication is completed, a droplet of DEME-TFSI is placed on the center of the device with a pipet to cover both the flake and liquid gate electrode. Figure 1e shows a schematic image of the device geometry. With this method, the ionic liquid only affects the carrier density of the contact region,

DOI: 10.1021/nl504750f
Nano Lett. 2015, 15, 1898−1903

while the main channel of the device is sealed by the hBN mask and remains largely unaffected.

Figure 3 shows the source-drain current through this device for different ionic liquid gate settings. As shown in Figure 3a, by changing the ionic liquid gate voltage V_{IL} from 2 V to −2 V, while sweeping the back-gate voltage, the device changes from balanced, ambipolar transistor behavior to strong p-type conduction, which indicates the enhancement of p-type contact when applying a favorable negative ionic liquid gate voltage. This effect is also shown in the $I-V$ curves with different ionic liquid gate voltages at fixed V_{BG} = −75 V (Figure 3b). Compared to V_{IL} = 0, the linearity of $I-V$ curve at V_{IL} = −2 V is greatly improved. This nearly ohmic contact rendered by high negative V_{IL} enables four-terminal resistivity and Hall measurements to extract contact resistance, intrinsic conductivity, and Hall mobility of this device. We note that all the measurements are done at a temperature ∼220 K, which is slightly above the freezing temperature of the liquid (∼200 K)[48] to minimize chemical reactions between the ionic liquid and contact leads.

On the basis of four-terminal measurements, the contact resistance, R_c, is extracted from the resistivity as $R_c = V_{ds}/I_{ds} - \rho \cdot l/w$, where l and w are the full sample length and width, respectively, and $\rho = (V_{xx}/I_{ds})/(l_{in}/w)$ with l_{in} as the length between the inner contacts, as shown in Figure 4a. From V_{IL} = 0 to −2 V, the contact resistance for V_{BG} = −75 V decreases by nearly a factor of 4, changing from 57 to 15 kΩ, which demonstrates the tunability of the contact resistance by the ionic liquid. We also plot conductivity as a function of V_{BG} for different V_{IL}, in Figure 4b. The conductivity reaches a maximum of 0.34 mS at V_{BG} = −75 V. Comparing different V_{IL}, the conductivity follows almost the same trace (Figure 3b) except for a small shift in threshold voltage. This confirms the transparency of the contacts and allows us to extract the intrinsic transport properties of the device.

The small change in conductivity for different V_{IL} also demonstrates that the device geometry introduced here allows independent tunability of the channel conductance and contact resistance. The ionic liquid gate only significantly influences the contact region, while the back gate controls the intrinsic conductivity of the device channel. When the ionic liquid is directly in contact with the semiconductor, the ions in the liquid and the free carriers in the semiconductor beneath the liquid form an equivalent capacitor with $c \sim 12\ \mu F/cm^2$,[48−51] which is ∼1000 times larger than for conventional dielectric gating with 300 nm thick SiO_2. In contrast, the relatively small shift of intrinsic conductivity corresponds to a capacitance of a top gate through a conventional dielectric. This smaller capacitance additionally rules out the possibility that ionic liquid penetrates below the top hBN mask.

The Hall effect is used to determine carrier density, n, and mobility, μ_H as a function of V_{BG}. At 220 K, we simultaneously measure V_{xx}, V_{xy}, and I_{DS} with an ac current bias of 0.5 μA. For the Hall measurement, the ionic liquid gate is set to −2 V to ensure the best p-type contact. The inset of Figure 4c shows $R_{xy} = V_{xy}/I_{DS}$ as a function of magnetic field at two selected back-gate voltages. The slope of the linear fit is equal to $1/(n_{2D}e)$, where n_{2D} is the carrier density, and e is the elementary charge. We combine measurements of carrier density and conductivity as a function of back-gate voltage to obtain the Hall mobility at different carrier densities. The nearly linear dependence of n_{2D} on V_{BG} corresponds to a capacitance per unit area c = 12 nF/cm^2. This value is in rough agreement with the capacitance expected for a parallel plate geometry with the bottom dielectric, 11.2 nF/cm^2 (25 nm thick hBN on top of 285 nm SiO_2), without taking into account the complexity of the device structure and possible influence from the top hBN and ionic liquid.

The Hall mobility extracted as a function of carrier density is plotted in Figure 4d, and μ_H > 600 cm^2/(V·s) is observed over a range of back-gate voltage, −75 to −40 V. For comparison, we also calculate the average field effect mobility from the conductivity in Figure 4b, assuming c = 12 nF/cm^2 for the same range of back-gate voltages (−75 to −40 V). We obtain μ_{FE} = 600 ± 80 cm^2/(V·s), which is in good agreement with the measured μ_H. For bulk WSe_2, hole mobility as high as ∼500 cm^2/(V·s) was measured,[8] and recent work on monolayer WSe_2 FETs reported 2-probe field-effect hole mobility up to ∼250 cm^2/(V·s) at room temperature.[34] In addition, at 77 K ionic liquid-gated graphene contacts to few-layer WSe_2 revealed Hall mobility up to ∼330 cm^2/(V·s).[35] For hBN-encapsulated MoS_2, recent work shows mobilities in the range of 100−300 cm^2/(V·s) at 200 K for 1- to 6-layer thick MoS_2.[30] The relatively high Hall mobility of the devices presented here supports our claim that encapsulation in hBN improves the performance of TMD devices with the help of ionic liquid gating that significantly improves the contact quality. This result highlights the potential for observing novel quantum transport phenomena in WSe_2.[52] Another merit of this geometry is that the hBN acts as a barrier to the disordered charges in ionic liquid and possible chemical reactions induced on the device surface during operation, which may also contribute to the improved mobility, similar to a previous report on hBN covered STO samples.[53]

We have presented a fabrication scheme to pick-up and transfer prepatterned hBN mask as a core technique to create 2D van der Waals heterostructures. The hBN can be patterned into arbitrary shapes to fit the needs of various experiments at the mesoscopic scale, and the robustness of this method allows multiple pick-ups and transfers required to fabrication complex heterostructures. The dry fabrication procedure maintains pristine 2D materials in multiple stacks without thermal annealing, so it can be applied to thermally sensitive materials while greatly reducing the amount of time to fabricate heterostructures. Both devices presented here demonstrate a high level of cleanliness and high mobility. Independent gating of the contact region by ionic liquid demonstrated in this Letter also provides a solution to the persistent contact difficulty of TMD devices. Enabled by this technique, we also report the highest Hall mobility to date in a few-layer WSe_2 device.

■ ASSOCIATED CONTENT

Supporting Information

hBN mask preparation and device fabrication details. This material is available free of charge via the Internet at http://pubs.acs.org.

■ AUTHOR INFORMATION

Corresponding Authors

*E-mail: joelwang@mit.edu.
*E-mail: yafang@mit.edu.
*E-mail: pjarillo@mit.edu.

Author Contributions

J.I.-J.W. and Y.Y. contributed equally to this work.

DOI: 10.1021/nl504750f
Nano Lett. 2015, 15, 1898−1903

Notes

The authors declare no competing financial interest.

■ ACKNOWLEDGMENTS

We acknowledge experimental assistance from Britton Baugher, Jason Luo, and Javier Sanchez-Yamagishi. Y.Y. has been primarily funded by ONR Young Investigator Award N00014-13-1-0610, and partly by the ONR GATE MURI and a Packard Fellowship. J.I-J.W has been primarily supported by the US DOE, BES Office, Division of Materials Sciences and Engineering under Award DE-SC0001819. J.I-J.W. was partially supported by a Taiwan Merit Scholarship TMS-094-1-A-001. This work made use of the MRSEC Shared Experimental Facilities supported by NSF under award No. DMR-0819762 and of Harvard's CNS, supported by NSF under Grant ECS-0335765.

■ REFERENCES

(1) Geim, A. K.; Grigorieva, I. V. *Nature* **2013**, *499*, 419.
(2) Novoselov, K. S.; Geim, A. K.; Morozov, S. V.; Jiang, D.; Zhang, Y.; Dubonos, S. V. I; Grigorieva, V.; Firsov, A. A. *Science* **2004**, *306*, 666−669.
(3) Zhang, Y.; Tan, Y.-W.; Stormer, H. L.; Kim, P. *Nature* **2005**, *438*, 201−204.
(4) Katsnelson, M. I.; Novoselov, K. S.; Geim, A. K. *Nat. Phys.* **2006**, *2*, 620−625.
(5) Young, A. F.; Kim, P. *Nat. Phys.* **2009**, *5*, 222−226.
(6) Young, A. F.; Sanchez-Yamagishi, J. D.; Hunt, B.; Choi, S. H.; Watanabe, K.; Taniguchi, T.; Ashoori, R. C.; Jarillo-Herrero, P. *Nature* **2013**, *505*, 528−532.
(7) Wang, Q. H.; Kalantar-Zadeh, K.; Kis, A.; Coleman, J. N. *Nat. Nanotechnol.* **2012**, *7*, 699.
(8) Podzorov, V.; Gershenson, M. E.; Kloc, C.; Zeis, R.; Bucher, E. *Appl. Phys. Lett.* **2004**, *84*, 3301.
(9) Radisavljevic, B.; Kis, A. *Nat. Mater.* **2013**, *12*, 815−820.
(10) Baugher, B. W. H.; Churchill, H. O. H.; Yang, Y.; Jarillo-Herrero, P. *Nano Lett.* **2013**, *13*, 4212.
(11) Zhang, Y. J.; Ye, J. T.; Yomogida, Y.; Takenobu, T.; Iwasa, Y. *Nano Lett.* **2013**, *13*, 3023−3028.
(12) Wang, H.; Yu, L.; Lee, Y.-H.; Shi, Y.; Hsu, A.; Chin, M. L.; Li, L.-J.; Dubey, M.; Kong, J.; Palacios, T. *Nano Lett.* **2012**, *12*, 4674−4680.
(13) Yin, Z.; Li, H.; Li, H.; Jiang, L.; Shi, Y.; Sun, Y.; Lu, G.; Zhang, Q.; Chen, X.; Zhang, H. *ACS Nano* **2012**, *6*, 74−80.
(14) Lopez-Sanchez, O.; Lembke, D.; Kayci, M.; Radenovic, A.; Kis, A. *Nat. Nanotechnol.* **2013**, *8*, 497.
(15) Zeng, H.; Liu, G.-B.; Dai, J.; Yan, Y.; Zhu, B.; He, R.; Xie, L.; Xu, S.; Chen, X.; Yao, W.; Cui, X. *Sci. Rep.* **2013**, *3*, 1608.
(16) Mak, K. F.; He, K.; Shan, J.; Heinz, T. F. *Nat. Nanotechnol.* **2012**, *7*, 494−498.
(17) Sallen, G.; Bouet, L.; Marie, X.; Wang, G.; Zhu, C. R.; Han, W. P.; Lu, Y.; Tan, P. H.; Amand, T.; Liu, B. L.; Urbaszek, B. *Phys. Rev. B* **2012**, *86*, 081301.
(18) Jones, A. M.; Yu, H.; Ghimire, N.; Wu, S.; Aivazian, G.; Ross, J. S.; Zhao, B.; Yan, J.; Mandrus, D.; Xiao, D. *Nat. Nanotechnol.* **2013**, *8*, 634.
(19) Jones, A. M.; Yu, H.; Ross, J. S.; Klement, P.; Ghimire, N. J.; Yan, J.; Mandrus, D. G.; Yao, W.; Xu, X. *Nat. Phys.* **2014**, *10*, 130−134.
(20) Baugher, B. W. H.; Churchill, H. O. H.; Yang, Y.; Jarillo-Herrero, P. *Nat. Nanotechnol.* **2014**, *9*, 262−267.
(21) Ross, J. S.; Klement, P.; Jones, A. M.; Ghimire, N. J.; Yan, J.; Mandrus, D. G.; Taniguchi, T.; Watanabe, K.; Kitamura, K.; Yao, W.; Cobden, D. H.; Xu, X. *Nat. Nanotechnol.* **2014**, *9*, 268−272.
(22) Pospischil, A.; Furchi, M. M.; Mueller, T. *Nat. Nanotechnol.* **2014**, *9*, 257−261.
(23) Zhang, Y. J.; Oka, T.; Suzuki, R.; Ye, J. T.; Iwasa, Y. *Science* **2014**, *344*, 725−728.
(24) Mak, K. F.; McGill, K. L.; Park, J.; McEuen, P. L. *Science* **2014**, *344*, 1489−1492.
(25) Dean, C. R.; Young, A. F.; Meric, I.; Lee, C.; Wang, L.; Sorgenfrei, S.; Watanabe, K.; Taniguchi, T.; Kim, P.; Shepard, K. L. *Nat. Nanotechnol.* **2010**, *5*, 722−726.
(26) Bolotin, K. I.; Sikes, K. J.; Jiang, Z.; Klima, M.; Fudenberg, G.; Hone, J.; Kim, P.; Stormer, H. L. *Solid State Commun.* **2008**, *146*, 351−355.
(27) Du, X.; Skachko, I.; Barker, A.; Andrei, E. Y. *Nat. Nanotechnol.* **2008**, *3*, 491−495.
(28) Mayorov, A. S.; Gorbachev, R. V.; Morozov, S. V.; Britnell, L.; Jalil, R.; Ponomarenko, L. A.; Blake, P.; Novoselov, K. S.; Watanabe, K.; Taniguchi, T. *Nano Lett.* **2011**, *11*, 2396−2399.
(29) Taychatanapat, T.; Watanabe, K.; Taniguchi, T.; Jarillo-Herrero, P. *Nat. Phys.* **2013**, *9*, 225−229.
(30) Cui, X. et al. arXiv:1412.5977 [cond-mat.mtrl-sci].
(31) Das, S.; Chen, H.-Y.; Penumatcha, A. V.; Appenzeller, J. *Nano Lett.* **2012**, *13*, 100−105.
(32) Liu, W.; Kang, J.; Sarkar, D.; Khatami, Y.; Jena, D.; Banerjee, K. *Nano Lett.* **2013**, *13*, 1983−1990.
(33) Chuang, S.; Battaglia, C.; Azcatl, A.; McDonnell, S.; Kang, J. S.; Yin, X.; Tosun, M.; Kapadia, R.; Fang, H.; Wallace, R. M.; Javey, A. *Nano Lett.* **2014**, *14*, 1337−1342.
(34) Fang, H.; Chuang, S.; Chang, T. C.; Takei, K.; Takahashi, T.; Javey, A. *Nano Lett.* **2012**, *12*, 3788−3792.
(35) Chuang, H.-J.; Tan, X.; Ghimire, N. J.; Perera, M. M.; Chamlagain, B.; Cheng, M. M.-C.; Yan, J.; Mandrus, D.; Tománek, D.; Zhou, Z. *Nano Lett.* **2014**, *14*, 3594−3601.
(36) Wang, L.; Meric, I.; Huang, P. Y.; Gao, Q.; Gao, Y.; Tran, H.; Taniguchi, T.; Watanabe, K.; Campos, L. M.; Muller, D. A.; Guo, J.; Kim, P.; Hone, J.; Shepard, K. L.; Dean, C. R. *Science* **2013**, *342*, 614−617.
(37) Zomer, P. J.; Guimarães, M. H. D.; Brant, J. C.; Tombros, N.; van Wees, B. J. arXiv:1403.0399 [cond-mat.mes-hall].
(38) Hunt, B.; Sanchez-Yamagishi, J. D.; Young, A. F.; Yankowitz, M.; LeRoy, B. J.; Watanabe, K.; Taniguchi, T.; Moon, P.; Koshino, M.; Jarillo-Herrero, P. *Science* **2013**, *340*, 1427−1430.
(39) Williams, J. R.; DiCarlo, L.; Marcus, C. M. *Science* **2007**, *317*, 638−641.
(40) Ozyilmaz, B.; Jarillo-Herrero, P.; Efetov, D.; Abanin, D.; Levitov, L.; Kim, P. *Phys. Rev. Lett.* **2007**, *99*, 166804.
(41) Stander, N.; Huard, B.; Goldhaber-Gordon, D. *Phys. Rev. Lett.* **2009**, *102*, 026807.
(42) Hernández, G. *Fabry-Perot Interferometers*; Cambridge University Press: New York, 1988; Vol. 3.
(43) Campos, L. C.; Young, A. F.; Surakitbovorn, K.; Watanabe, K.; Taniguchi, T.; Jarillo-Herrero, P. *Nat. Commun.* **2012**, *3*, 1239.
(44) Rickhaus, P.; Maurand, R.; Liu, M.-H.; Weiss, M.; Richter, K.; Schönenberger, C. *Nat. Commun.* **2013**, *4*, 2342.
(45) Grushina, A. L.; Ki, D.-K.; Morpurgo, A. F. *Appl. Phys. Lett.* **2013**, *102*, 223102.
(46) Xia, F.; Perebeinos, V.; Lin, Y.-m.; Wu, Y.; Avouris, P. *Nat. Nano.* **2011**, *6*, 179−184.
(47) Hwang, E. H.; Adam, S.; Sarma, S. D. *Phys. Rev. Lett.* **2007**, *98*, 186806.
(48) Ye, J. T.; Zhang, Y. J.; Akashi, R.; Bahramy, M. S.; Arita, R.; Iwasa, Y. *Science* **2012**, *338*, 1193−1196.
(49) Ohno, H. *Electrochemical Aspects of Ionic Liquids*; John Wiley & Sons, 2011.
(50) Ueno, K.; Nakamura, S.; Shimotani, H.; Ohtomo, A.; Kimura, N.; Nojima, T.; Aoki, H.; Iwasa, Y.; Kawasaki, M. *Nat. Mater.* **2008**, *7*, 855−858.
(51) Ye, J. T.; Inoue, S.; Kobayashi, K.; Kasahara, Y.; Yuan, H. T.; Shimotani, H.; Iwasa, Y. *Nat. Mater.* **2010**, *9*, 125−128.
(52) Li, X.; Zhang, F.; Niu, Q. *Phys. Rev. Lett.* **2013**, *110*, 066803.
(53) Gallagher, P.; Lee, M.; Petach, T. A.; Stanwyck, S. W.; Williams, J. R.; Watanabe, K.; Taniguchi, T.; Goldhaber-Gordon, D. *arXiv* 2014, *arXiv:1410.3034*.

DOI: 10.1021/nl504750f
Nano Lett. 2015, 15, 1898−1903